POLITECNICO DI TORINO Repository ISTITUZIONALE

Estimating geometric tortuosity of saturated rocks from micro-CT images using percolation theory

Original

Estimating geometric tortuosity of saturated rocks from micro-CT images using percolation theory / Panini, Filippo; Ghanbarian, Behzad; Salina Borello, Eloisa; Viberti, Dario. - In: TRANSPORT IN POROUS MEDIA. - ISSN 0169-3913. - ELETTRONICO. - 151:(2024), pp. 1579-1606. [10.1007/s11242-024-02085-w]

Availability:

This version is available at: 11583/2988348 since: 2024-05-30T14:06:31Z

Publisher: Springer

Published

DOI:10.1007/s11242-024-02085-w

Terms of use:

This article is made available under terms and conditions as specified in the corresponding bibliographic description in the repository

Publisher copyright

Springer postprint/Author's Accepted Manuscript

This version of the article has been accepted for publication, after peer review (when applicable) and is subject to Springer Nature's AM terms of use, but is not the Version of Record and does not reflect post-acceptance improvements, or any corrections. The Version of Record is available online at: http://dx.doi.org/10.1007/s11242-024-02085-w

(Article begins on next page)

Vol. 43, No. 1 Jan. 2 0 1 3

JOURNAL OF UNIVERSITY OF SCIENCE AND TECHNOLOGY OF CHINA

Article ID: 0253-2778(2013)01-0001-14

Planetary landing: Modelling and control of the propulsion descent

Canuto Enrico¹, Molano-Jimenez Andrés¹, Perez-Montenegro Carlos¹, Malan Stefano¹, Martella Paolo²

(1. Politecnico di Torino, Dipartimento di Automaticae Informatica, Corso Duca degli Abruzzi 24, 10129 Torino, Italy,
 2. Thales Alenia Space Italia, Strada Antica di Collegno 253, 10135, Torino, Italy)

Abstract: In the propulsion phase, after parachute release, of landing on Mars or the Moon, horizontal motion is obtained by tilting the axial thrust so that it aligns either to the negative velocity vector (gravity turn) or to the requested acceleration vector. The latter strategy is assumed here, as it allows pinpoint landing. As such, tilt angles (pitch and yaw) become proportional to the horizontal acceleration. Instead of designing a hierarchical guidance and control in which horizontal acceleration becomes the attitude control target, a unique control system was designed based on the fourth order dynamics from angular acceleration to position. It is shown that the combined dynamics can be (quasi) input-state linearized except for the nonlinear factor of the tilt angles (the axial thrust imposed by vertical braking). It is also shown that the control design around the reference trajectory (tilt and position) can only exploit a partial input-state linearization, but internal stability can be proved. Stability is also proved in the presence of an external disturbance dynamics that is not stabilizable. The paper is restricted to closed-loop control strategies, and their effectiveness is proved through Monte Carlo simulations.

Key words: planetary landing; powered descent; closed-loop control; attitude control; position control **CLC number:** TH811 **Document code:** A doi:10.3969/j.issn.0253-2778.2013.01.001

Citation: Canuto Enrico, Molano-Jimenez Andrés, Perez-Montenegro Carlos, et al. Planetary landing: Modelling and control of the propulsion descent[J]. Journal of University of Science and Technology of China, 2013, 43(1): 1-14.

行星着陆 ——推进下降过程的建模与控制

Canuto Enrico¹, Molano-Jimenez Andrés¹, Perez-Montenegro Carlos¹, Malan Stefano¹, Martella Paolo²

> (1. 都灵理工大学自动化与电子信息科学系,都灵 10129,意大利; 2. 阿莱尼亚航天公司,Strada Antica di Collegno 253,都灵 10135,意大利)

摘要:登陆火星或月球时,释放降落伞后进入推进阶段,通过轴向推力倾斜实现水平方向运动,能够与速度矢

Received: 2012-09-06; Revised: 2012-10-31

Biography: Canuto Enrico (corresponding author), male, born in 1945, Professor. E-mail: enrico. canuto@polito. it

量(重力)的相反方向一致或与需要的加速度方向保持一致.后一种策略能实现精确着陆,在该策略下,倾斜角(俯仰角和偏转角)与水平加速度成正比.这种策略并未采用以水平加速度为姿态控制目标的递阶导航与控制方案,而是基于角加速度对位置作用的四阶动力学特性设计了一个独特的控制系统.除去倾斜角的非线性因素(垂直制动规定的轴向推力)后,系统综合动力学方程能够实现(准)输入-状态线性化.论文同时表明:一方面,基于参考轨迹(倾斜角和位置)的控制器设计仅能实现部分输入-状态线性化;另一方面,系统的内部稳定性可以证明.即使存在不可镇定的外部干扰动力学模态时,仍能确保系统稳定性.蒙特卡洛仿真验证了闭环控制策略的有效性.

关键词:行星着陆:有动力下降:闭环控制:姿态控制:位置控制

0 Introduction

Propulsion guidance and control of a landing vehicle, during the terminal phase (descent) after parachute release until thrusters are switched off, is usually obtained by appropriate orientation of the main engines in charge of vehicle braking. The thruster assembly can only provide a three degreesof-freedom command (braking, pitch and yaw torque) plus spin damping (around the vehicle symmetry axis). Thrust may be oriented either opposite to the current speed (gravity-turn maneuver^[1-5]) or along the desired acceleration (Apollo-like guidance [6-12]). In Apollo-like guidance, the centre-of-mass (CoM) trajectory is interpolated between initial and kinematic constraints through a 3D polynomial, thus becoming suitable for pinpoint landing^[11]. Polynomial degree depends on the constraint size: a quartic polynomial is capable of respecting initial and final positions and rates, but only final not initial, acceleration. A quintic polynomial satisfies also initial acceleration. The guidance of the MSL (Mars Science Laboratory[8,13]), which successfully landed on August 2012, followed a modified Apollo guidance law using a quintic polynomial law.

The majority of the above studies are concentrated on the guidance problem, and the relevant issues of adaptive guidance to contrast disturbance^[14], altitude measurement errors and target site modification. From this standpoint simple feedback laws around the guidance trajectory are kept as sufficient (see for instance the sliding mode control strategy in Ref. [15]). They are completed by an attitude control

around the attitude reference imposed by a guidance law^[7] which aligns the vehicle axis either to the negative velocity vector or to the acceleration vector.

Here the overall powered descent control will be studied combining CoM and tilt (pitch and yaw) dynamics, as the latter provides the acceleration for the horizontal motion (a similar approach addressing quad-rotors control is Ref. [16]). The approach as in Ref. [16] is to obtain an input-state linearized dynamics[17] from angular acceleration to (horizontal) position (fourth order in each degreeof-freedom), and to design guidance, navigation and control based on the same combined state equations as suggested by Embedded Model Control^[18-23]. The paper, restricted to modeling and control, shows that a complete linearization is not viable as the nonlinear and variable axial thrust acceleration is the inherent (positive) gain ensuring controllability of a fourth order series of integrators. Moreover, but less severe, the gain connects both horizontal axes and, further, an oscillatory zero dynamics sets up because of a feed-forward connection between command torques and horizontal forces (due to slanted thrusters). Input-state linearization is instead viable on the separated CoM and attitude state equations. Control is designed by assuming input-state linearization, and internal stability of the tracking error equation is proved. Actually tracking error is proved to be bounded also in the presence of an external disturbance dynamics that is not stabilizable. Indeed, under perfect state knowledge, the output of the disturbance dynamics can be exactly cancelled by the control law. Instead, in the presence of measurement errors coming from navigation (not treated in the paper), the disturbance can only be cancelled less a bounded error (actually a prediction error) entering the prediction error equation as in Refs. [19-20,22]. The effectiveness of the design is proved by Monte Carlo simulations.

1 Planetary descent dynamics

1.1 Assumptions

The dynamics of a landing body after parachute release is derived in the Appendix under these assumptions:

- (I) position and velocity coordinates are defined in a planet-fixed local-vertical-local-horizontal frame R_l ;
- (Π) CoM trajectory is actuated by body-fixed quasi-axial thrusters, which implies that horizontal motion can only be obtained by tilting the body axis \vec{k}_b ;
- (\blacksquare) thrusters modulate the body tilt angles (pitch θ and yaw φ) as requested by CoM guidance and control;
- (N) tilt angles are 1 and 2 Euler angles of the $\{1,2,3\}$ body-to-local transformation R_b^l ; the third angle ψ (spin) is absorbed as a parameter of the input matrices;
- (V) the body is de-spun by a specific thruster assembly;
- (VI) horizontal and vertical dynamics are treated as decoupled in view of control design;
- (\mathbb{W}) tilt angles are bounded (a vertical cone with a semi-aperture of about $\pi/4$) by sensor limitations (radar, camera), the spin angle ψ is arbitrary;
 - (\mathbb{I}) the body is axisymmetric with inertia matrix $J = \text{diag}(J_x, J_x, J_z)$ (1)

Trigonometric notations are simplified to $c_x = \cos x$, $s_x = \sin x$ and $t_x = \tan x$, x being a generic angle.

1.2 Reference frames

The equations of flight and attitude of a body over a rotating planet are recalled in the Appendix on the basis of the three frames of reference as in Fig. 1.

The inertial frame $R_p = (C_p, \vec{i}_p, \vec{j}_p, \vec{k}_p)$ is

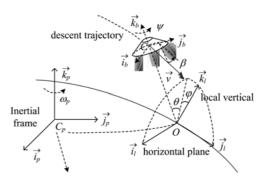


Fig. 1 Frames of reference

centered on the planet CoM C_p , the co-rotating local vertical local horizontal frame $R_l = (O, \vec{i}_l, \vec{j}_l, \vec{k}_l)$ (briefly local frame) is centered on the fixed surface point O and has vertical direction \vec{k}_l , the body frame $R_b = (C, \vec{i}_b, \vec{j}_b, \vec{k}_b)$ is centered on the body CoM C and the axial direction \vec{k}_b is directed opposite to the velocity vector \vec{v} .

The body to local and the local to planet transformations are denoted by R_b^l and R_b^p respectively.

1.3 Attitude dynamics and input-state linearization

We start from the attitude dynamics which acts as the actuator of the horizontal motion. Input-state linearization as in Ref. [17] is performed given a nonlinear function $q(\theta)$ of the attitude vector θ ; then a specific Euler angle sequence (triple) is looked for which allows linearization and command decoupling between tilt and spin in the case of axisymmetric inertia as in (1). The selected triple is $\{1,2,3\} = \{\varphi,\theta,\psi\}$. Full command decoupling (block-diagonal) occurs if only the spin rate, and not the spin angle ψ , is controlled, which is the case when body orientation is of no concern.

1.3.1 Linearization

Consider the kinematic and dynamic equations of the triple $\boldsymbol{\theta} = \begin{bmatrix} \theta_1 & \theta_2 & \theta_3 \end{bmatrix}^T$ of Euler angles that define the body-to-local transformation $R_b^I(\boldsymbol{q})$, and of the corresponding angular rate (in body coordinates) $\boldsymbol{\omega}_b$. They are driven by the command torque \boldsymbol{M} , and hold

$$\begin{vmatrix}
\dot{\boldsymbol{\theta}} = A_{\theta}(\boldsymbol{\theta}) \, \boldsymbol{\omega}_{b} \\
\dot{\boldsymbol{\omega}}_{b} = J^{-1} (\boldsymbol{M} + \boldsymbol{M}_{d}) - J^{-1} (\boldsymbol{\omega}_{b} \times \boldsymbol{J} + \dot{\boldsymbol{J}}) \, \boldsymbol{\omega}_{b}
\end{vmatrix} (2)$$

Eq. (2) correspond to the following nonlinear

equation to-be input-state linearized

$$\dot{\mathbf{x}}(t) = \mathbf{f}(\mathbf{x}) + G(\mathbf{x})(\mathbf{u} + \mathbf{d})
\mathbf{x} = \begin{bmatrix} \mathbf{\theta}^{\mathrm{T}} & \mathbf{\omega}_{b}^{\mathrm{T}} \end{bmatrix}^{\mathrm{T}}, \quad \mathbf{u} = \mathbf{M}, \quad \mathbf{d} = \mathbf{M}_{d}
\mathbf{f}(\mathbf{x}) = \begin{bmatrix} A_{\theta}(\mathbf{\theta}) \mathbf{\omega}_{b} \\ -J^{-1}(\mathbf{\omega}_{b} \times J + \dot{J}) \mathbf{\omega}_{b} \end{bmatrix}
G(\mathbf{x}) = \begin{bmatrix} 0 \\ J^{-1} \end{bmatrix}$$
(3)

In Eq. (2) \mathbf{M}_d includes aerodynamic torques and thruster errors, $\dot{\mathbf{J}}$ is the inertia derivative accounting for propellant consumption, and $A_{\theta}(\boldsymbol{\theta})$ depends on the selected Euler triple. The set Ω of the admissible $\boldsymbol{\theta}$, to be respected by the attitude control, must guarantee that $A_{\theta}(\boldsymbol{\theta}): \Omega \to R^3$ is invertible in Ω . The following Theorem proves under which conditions (2) can be input-state linearized.

Theorem 1.1 Given Eq. (2), consider the smooth transformation $q = q(\theta) : \Omega \rightarrow R^3$ and assume that the Jacobian $Q(\theta) = dq(\theta)/d\theta$ is invertible in Ω . Then define the angular rate $\omega = S(\theta) \omega_b$ with the equality $S(\theta) = Q(\theta) A_{\theta}(\theta)$.

$$\begin{bmatrix} \dot{\mathbf{q}} \\ \dot{\boldsymbol{\omega}} \end{bmatrix}(t) = \begin{bmatrix} 0 & \mathbf{I} \\ 0 & 0 \end{bmatrix} \begin{bmatrix} \mathbf{q} \\ \boldsymbol{\omega} \end{bmatrix}(t) + \begin{bmatrix} 0 \\ \mathbf{I} \end{bmatrix} \boldsymbol{\alpha}(t)
\boldsymbol{\alpha}(t) = L(\boldsymbol{\theta}) (\mathbf{M} + \mathbf{M}_d) + m(\boldsymbol{\theta}, \boldsymbol{\omega}_b)$$
(4)

where $L(\boldsymbol{\theta}) = S(\boldsymbol{\theta}) J^{-1}$ must be invertible in Ω .

Proof The proof follows because $L(\boldsymbol{\theta})$ is invertible in Ω , owing to Q and A_{θ} being invertible. The term $m(\boldsymbol{\theta}, \boldsymbol{\omega}_{\theta})$, playing the role of a known disturbance^[18] holds

$$m(\boldsymbol{\theta}, \boldsymbol{\omega}_b) = -L(\boldsymbol{\theta})(\boldsymbol{\omega}_b \times J\boldsymbol{\omega}_b + \dot{J}\boldsymbol{\omega}_b) + \sum_{k=1}^{3} S_k(\boldsymbol{\theta}) \boldsymbol{\omega}_b \boldsymbol{\omega}_b^{\mathrm{T}} \boldsymbol{a}_{0k}(\boldsymbol{\theta})$$
 (5)

where $S_k(\boldsymbol{\theta}) = \partial S(\boldsymbol{\theta})/\partial \theta_k$, and $\boldsymbol{a}_{\ell k}(\boldsymbol{\theta})$ is the k-th row of A_{θ} . The state transformation T that defines the new state vector \mathbf{z} of the linearized equation holds

$$z = T(x) = \begin{bmatrix} q(\theta) \\ S(\theta) \omega_b \end{bmatrix}$$

$$z = \begin{bmatrix} q \\ \omega \end{bmatrix}, x = \begin{bmatrix} \theta \\ \omega \end{bmatrix}$$
(6)

The resulting linear state equation which is the same as Eq. (4):

$$\dot{\mathbf{z}}(t) = \mathbf{A}\mathbf{z}(t) + \mathbf{B}\mathbf{\alpha}(t) \tag{7}$$

where α has been defined in Eq. (4), and the matrices are

$$\mathbf{A} = \begin{bmatrix} 0 & \mathbf{I} \\ 0 & 0 \end{bmatrix}, \ \mathbf{B} = \begin{bmatrix} 0 \\ \mathbf{I} \end{bmatrix} \tag{8}$$

The pair (A, B) is controllable and has a multivariate companion form.

1.3.2 Command decoupling

The next step is to find the right Euler sequence satisfying Theorem 1. The introductory assumption fixing a bounded tilt $\{\varphi,\theta\}$ of \vec{k}_b with respect to \vec{k}_l , and an arbitrary spin ψ , suggests the following admissible set:

 $\Omega = \{ \sqrt{\varphi^2 + \theta^2} \leqslant q_{\text{max}} < \pi/2, \ \psi \ \text{any} \}$ (9) Since given a Tayt-Brian sequence $\{\theta_1, \theta_2, \theta_3\}$ -each rotation is about a different Cartesian axis -, $A_{\theta}(\theta)$ becomes singular when $\theta_2 = \pm \pi/2$, only the following sequences satisfy Theorem 1, namely

 $\{1,2,3\},\{3,2,1\},\{2,1,3\},\{3,1,2\}$ (10) Moreover, keeping the exchange between 1 and 2 not significant, the choice, restricted to the former two sequences in Eq. (10), calls for further criteria. A first criterion is to decouple tilt and spin commands. That amounts imposing $L(\theta)$ in Eq. (4) to become block-triangular as follows:

$$L(\boldsymbol{\theta}) = \begin{bmatrix} L_{12}(\boldsymbol{\theta})_{2\times 2} & 0 \\ L_{123}(\boldsymbol{\theta}) & L_{3}(\boldsymbol{\theta})_{1\times 1} \end{bmatrix}$$

$$\boldsymbol{\theta} = \begin{bmatrix} \varphi & \theta & \psi \end{bmatrix}^{T}$$
(11)

Full decoupling would call for L_{123} (θ) = 0. Only $\{1,2,3\}$ satisfies Eq. (11) as the following Lemma states.

Lemma 1.1 Given $Q(\theta) = I$ and J in (1), $L(\theta) = A_{\theta}(\theta) J^{-1}$ is block-triangular only for $\{1, 2, 3\}$.

Proof First consider $\{1, 2, 3\}$ and write $A_{\theta}(\theta)$ as

$$A_{\theta}(\boldsymbol{\theta}) = \begin{bmatrix} 1/c_{\theta} & 0 & 0\\ 0 & 1 & 0\\ -t_{\theta} & 0 & 1 \end{bmatrix} Z(\boldsymbol{\psi})$$
 (12)

which is in the form of Eq. (11); the form is not changed by J^{-1} . Consider now $\{3,2,1\}$, and keep the same $\boldsymbol{\theta}$ as in Eq. (11). $A_{\theta}(\boldsymbol{\theta})$, written as

$$A_{\theta}(\boldsymbol{\theta}) = \begin{bmatrix} 1 & 0 & t_{\theta} \\ 0 & 1 & 0 \\ 0 & 0 & 1/c_{\theta} \end{bmatrix} X(\varphi) \tag{13}$$

does not respect Eq. (11).

A further advantage of $\{1,2,3\}$ versus $\{3,2,1\}$ is that the series of attitude and CoM dynamics can be partially input-state linearized only in the former case. The body-to-local transformation R_b^l of $\{1,2,3\}$ is

$$R_b^l = R(\varphi, \theta) Z(\psi), Z(\psi) = \begin{bmatrix} Z_{12}(\psi) & 0 \\ 0 & 1 \end{bmatrix} (14)$$

with

$$R(\varphi,\theta) = \begin{bmatrix} c_{\theta} & 0 & s_{\theta} \\ s_{\theta}s_{\varphi} & c_{\varphi} & -c_{\theta}s_{\varphi} \\ -s_{\theta}c_{\varphi} & s_{\varphi} & c_{\theta}c_{\varphi} \end{bmatrix}$$

$$Z_{12}(\psi) = \begin{bmatrix} c_{\psi} & -s_{\psi} \\ s_{\psi} & c_{\psi} \end{bmatrix}$$

$$(15)$$

1.3.3 Body de-spinning

A specific orientation of the body is not usually required: only de-spinning just after thruster firing is mandatory. Hence ψ need not be directly controlled: Only ω_{bz} must be driven to approach zero. With the help of Eq. (12), the state z in Eq. (7) reduces to five components.

$$\mathbf{z} = \begin{bmatrix} q_x & q_y \mid \omega_x & \omega_y \mid \omega_{bz} \end{bmatrix}^{\mathrm{T}} = \begin{bmatrix} \mathbf{q}^{\mathrm{T}} & \mathbf{\omega}_x^{\mathrm{T}} & \omega_{bz} \end{bmatrix}$$
(16)

and the transformation T in Eq. (7) becomes

$$T = \begin{bmatrix} \mathbf{q}^{T}(\varphi, \theta) & \begin{bmatrix} \omega_{bx} & \omega_{by} \end{bmatrix} S^{T}(\mathbf{\theta}) & \omega_{bz} \end{bmatrix}^{T} (17)$$
 with

$$\mathbf{q}(\varphi,\theta) = \begin{bmatrix} q_x \\ q_y \end{bmatrix} (\varphi,\theta) = \begin{bmatrix} c_{\theta} s_{\varphi} \\ s_{\theta} \end{bmatrix}$$

$$S(\mathbf{\theta}) = Q_{12} (\varphi,\theta) Z_{12} (\psi)$$

$$(18)$$

and

$$Q_{12}(\varphi,\theta) = \begin{bmatrix} \frac{\partial q_x}{\partial \varphi} & \frac{1}{c_{\theta}} & \frac{\partial q_x}{\partial \theta} \\ \frac{\partial q_y}{\partial \varphi} & \frac{1}{c_{\theta}} & \frac{\partial q_y}{\partial \theta} \end{bmatrix} = \begin{bmatrix} c_{\varphi} & -s_{\theta} s_{\varphi} \\ 0 & c_{\theta} \end{bmatrix}$$
(19)

Notice that ω_x is just 2D. Since $L_{123}(\theta) = 0$ in Eq. (17), $L(\theta)$ in Eq. (11) becomes block-diagonal, and the spin equation.

$$\dot{\psi}(t) = -t_{\theta}(t) \omega_{bx}(t) + \omega_{bz}(t) \tag{20}$$

comes out of Eq. (7). Assuming that $\omega_{bx} \rightarrow 0$, $\dot{\psi}$ just accounts for the yaw rate ω_{bx} (expressing a change of direction) of a pitch-inclined body with $t_{\theta} \neq 0$. The yaw rate ω_{bx} and the pitch θ are brought to zero close to landing, when vertical alignment of

the body axis is mandatory.

1.4 Overall dynamics

CoM and attitude dynamics are now separately written assuming a specific attitude function $q(\varphi, \theta)$ that drives the horizontal trajectory. CoM dynamics is obtained as a flat planet simplification of the entry equations, that are recalled in the Appendix. Both dynamics, if separated, can be input-state linearized.

1.4.1 CoM dynamics

Start from Eq. (75) in the Appendix, and assume that the attitude sequence {1,2,3} has been selected. Define the new position, velocity, thrust acceleration and disturbance coordinates as follows:

$$\begin{bmatrix}
\mathbf{x} \\
z
\end{bmatrix} = \begin{bmatrix}
\mathbf{P} & 0 \\
0 & 1
\end{bmatrix} \mathbf{r}_{l}, \begin{bmatrix}
\mathbf{v} \\
v_{z}
\end{bmatrix} = \begin{bmatrix}
\mathbf{P} & 0 \\
0 & 1
\end{bmatrix} \mathbf{v}_{l}$$

$$\begin{bmatrix}
\mathbf{a}_{bx} \\
a_{bz}
\end{bmatrix} = \begin{bmatrix}
\mathbf{P} & 0 \\
0 & 1
\end{bmatrix} \mathbf{a}_{b}, \begin{bmatrix}
\mathbf{d}_{x} \\
d_{z}
\end{bmatrix} = \begin{bmatrix}
\mathbf{P} & 0 \\
0 & 1
\end{bmatrix} \mathbf{d}_{l}$$
(21)

where the permutation matrix P is defined by

$$\mathbf{P} = \begin{bmatrix} 0 & -1 \\ 1 & 0 \end{bmatrix} \tag{22}$$

Applying Eq. (22) to Eq. (14) and using Eqs. (18) and (19) provides the equality.

$$\begin{bmatrix} \mathbf{P} & 0 \\ 0 & 1 \end{bmatrix} R(\varphi, \theta) Z(\psi) \begin{bmatrix} \mathbf{P}^{-1} & 0 \\ 0 & 1 \end{bmatrix} = \begin{bmatrix} S(\boldsymbol{\theta}) & \boldsymbol{q} \\ -B_z(\boldsymbol{\theta}) & c \end{bmatrix}$$
(23)

where

$$B_{\varepsilon}(\boldsymbol{\theta}) = \begin{bmatrix} s_{\varphi} & s_{\theta}c_{\varphi} \end{bmatrix} Z_{12}(\boldsymbol{\psi})$$

$$c(t) = c_{\theta}c_{\varphi}$$
(24)

Using Eq. (23), Eq. (75) in the Appendix is rewritten by splitting horizontal and vertical dynamics as follows:

$$\dot{\mathbf{x}}(t) = \mathbf{v}_{x}(t)
\dot{\mathbf{v}}_{x}(t) = \mathbf{a}_{x}(t)
\dot{\mathbf{z}}(t) = \mathbf{v}_{z}(t)
\dot{\mathbf{v}}_{z}(t) = \mathbf{u}_{z}(t)$$
(25)

where Eqs. (23) and (24) have been used to find

$$u_{z}(t) = a_{z}(t) - B_{z}(\theta) a_{hx}(t) - g + d_{z}(t)$$

$$a_{z}(t) = ca_{hz}(t)$$
(26)

and

$$\begin{aligned}
\mathbf{a}_{x}(t) &= a_{bx}(t)\mathbf{q}(t) + \mathbf{a}_{q}(t) \\
\mathbf{a}_{q}(t) &= S(\mathbf{\theta})\mathbf{a}_{bx}(t) + \mathbf{d}_{x}(t)
\end{aligned} (27)$$

Input-output linearization is ensured by the next Theorem.

Theorem 1.2 Eq. (25) together with Eq. (26) is input-state linearizable, if and only if

$$a_{bz}(t) = \frac{u_z(t) + g - d_z(t) + B_z(\theta) a_{bx}(t)}{c(t)} > 0$$
(28)

Proof If $a_{bz}(t) > 0$, an acceleration command a_x in Eq. (27) can be constructed such that

$$\mathbf{q}(t) = a_{bx}^{-1}(t) (\mathbf{a}_{x}(t) - \mathbf{S}(\mathbf{\theta}) \mathbf{a}_{bx}(t) - \mathbf{d}_{x}(t))$$
(29)

which proves sufficiency. Allowing a_{bz} (t) to become negative would impede Eq. (29), thus proving necessity. Eq. (28) is satisfied if

$$c(t) > 0 \tag{30}$$

which follows from Eq. (9), and if

$$u_z(t) > -(g - d_z(t) + B_z(\theta) a_{bx}(t))$$
 (31)

Inequality (31) can be simplified and completed as follows:

$$-1+\delta < \mu(t) = \frac{u_{\varepsilon}(t)}{g} < 1, \ 0 \leqslant \delta \ll 1 \ (32)$$

having assumed that $|d_z - B_z(\theta) a_{bx}|$ is a small fraction δ of $g \cong 3.7 \text{ m/s}^2$ (Mars), and imposing that the braking acceleration is smaller than gravity. This is justified by the negligible vertical aerodynamic acceleration d_z and by a_{bx} which is small fraction of g as proven by Eq. (42). Observe that Eq. (32) allows the vehicle braking ($u_z > 0$) and accelerating ($u_z < 0$). Acceleration may become mandatory for avoiding obstacles and pinpointing the target site.

Input-state linearization cannot be obtained in the same manner for $\{3,2,1\}$. In the case of $\{1,2,3\}$ the tilt angles $\{\varphi,\theta\}$ combine to move a body along orthogonal directions, and opposite directions are obtained by changing the angle sign while keeping the maximum stroke less than $2q_{\max}$. In $\{3,2,1\}$ the heading angle ψ fixes the direction, which requires a π stroke to move backward. Horizontal motion along the given direction is driven by θ .

1.4.2 Attitude dynamics

Using Eqs. (4), (5) and (17), attitude

equations become

$$\begin{vmatrix}
\dot{\mathbf{q}}(t) &= \mathbf{\omega}_{x}(t) \\
\dot{\mathbf{\omega}}_{x}(t) &= \mathbf{\alpha}_{x}(t) \\
\dot{\mathbf{\omega}}_{x} &= \alpha_{x}(t)
\end{vmatrix}$$
(33)

with the expressions

$$\boldsymbol{\alpha}_{x} = J_{x}^{-1} S(\boldsymbol{\theta}) \mathbf{M}_{x} + J_{x}^{-1} S(\boldsymbol{\theta}) \mathbf{M}_{dx} + \boldsymbol{m}_{x}(\boldsymbol{\theta}, \boldsymbol{\omega}_{b})$$

$$\boldsymbol{m}_{x}(\boldsymbol{\theta}, \boldsymbol{\omega}_{b}) = J_{x}^{-1} S(\boldsymbol{\theta}) ((J_{z} - J_{x}) \boldsymbol{\omega}_{bz} P - \dot{J}_{x} I) \boldsymbol{\omega}_{bx} + \dot{\boldsymbol{\psi}} S(\boldsymbol{\theta}) \boldsymbol{\omega}_{bx} + \sum_{k=1}^{2} \frac{\partial Q_{12}(\boldsymbol{\theta})}{\partial \theta_{1}} Z_{12}(\boldsymbol{\psi}) \boldsymbol{\omega}_{bx} \boldsymbol{\omega}_{bx}^{T} \boldsymbol{q}_{k}(\boldsymbol{\theta})$$

$$\boldsymbol{\alpha}_{z} = J_{z}^{-1} (-\boldsymbol{\omega}_{z} \dot{\boldsymbol{J}}_{z} + \boldsymbol{M}_{dz} + \boldsymbol{M}_{z})$$
(34)

In Eq. (34) \mathbf{q}_k is the k-th row of \mathbf{Q}_{12} .

The following corollary is a restatement of Theorem 1.1.

Corollary 1.1 Eqs. (33) and (34) are inputstate linearized.

Theorem 1.2 and Corollary 1.1 suggest that the control algorithms computing \mathbf{a}_x in Eq. (29) and \mathbf{a}_x in Eq. (33) must be designed in a hierarchical way as in Refs. [7-8,14]. A further reason would come by the difficulties of combining Eqs. (25) and (33). Indeed the combination becomes not linearizable, and shows an oscillatory zero dynamics. The main result of this paper is a control design based on the combined dynamics, together with a stability proof and simulated results.

1.5 Properties of the combined dynamics

CoM and attitude dynamics Eqs. (25) and (33) are now combined in a unique dynamics: the process passes through the definition of the thruster assembly and of the dispatching law. Only the assembly in charge of the axial thrust F_{bz} and of the tilt torques M_x and M_y is treated. It is shown that the combined dynamics cannot be input-state linearized, unless the second order derivative of the axial acceleration a_{bz} is defined, which is deemed useless. A linear time-varying equation results, together with an oscillatory zero dynamics. The main result is a stable and effective control design for such a dynamics.

1.5.1 Thruster assembly

Combination of CoM and attitude dynamics is

obtained by relating \mathbf{a}_q in Eq. (27) to \mathbf{a}_x in Eq. (33), which needs to define the thruster assembly. Consider for simplicity's sake four thrusters k=1, 2,3,4 forming a cone with a semi-aperture of $\beta \cong 0.35$ rad (see Fig. 1). The application points have body coordinates $\mathbf{a}_k = [\pm r \pm r - h]$, with $h \ll r$. The matrix thrust-to-force/torque, free of M_z , holds

$$\begin{bmatrix} F_{bx} \\ F_{by} \\ \vdots \\ F_{bz} \\ M_{x} \\ M_{y} \end{bmatrix} = \begin{bmatrix} B_{tx} \\ \vdots \\ B_{tz} \end{bmatrix} u_{t} = \begin{bmatrix} s & 0 & -s & 0 \\ 0 & s & 0 & -s \\ \vdots & \vdots & \vdots & \vdots \\ c & c & c & c & c \\ 0 & -\sigma & 0 & \sigma \\ \sigma & 0 & -\sigma & 0 \end{bmatrix} \begin{bmatrix} u_{t1} \\ u_{t2} \\ u_{t3} \\ u_{t4} \end{bmatrix}$$
(35)

where u_t is the thrust vector and

$$s = \sin \beta, \ c = \cos \beta$$

 $\sigma = r\cos \beta - h\sin \beta \cong r\cos \beta$ (36)

and c must not be confused with the symbol in Eq. (24). The next Lemma is immediate.

Lemma 1.2 The matrix in Eq. (35) has rank 3, which implies that only three components are controllable.

The last three components in Eq. (35), the axial force F_{bz} and the tilt torques M_x and M_y are of concern. A dispatching law, ensuring a thrust vector $\mathbf{u}_t > 0$ must be provided. To this end, the torque components are written as

$$F_{bz} > 0$$
, $M_x = M_{x+} - M_{x-}$, $M_{x+} \ge 0$, $M_{x-} \ge 0$
 $M_y = M_{y+} - M_{y-}$, $M_{y+} \ge 0$, $M_{y-} \ge 0$

$$(37)$$

The following Theorem, easy to be proved, is a version of an unpublished Theorem proved by one of the authors at the times of the early GOCE design^[21].

Theorem 1.3 A dispatching strategy ensuring $u_t > 0$ is

$$u_{t} = \frac{1}{4c} \begin{bmatrix} 1 & 0 & \gamma \\ 1 & 0 & 0 \\ 1 & 0 & 0 \\ 1 & \gamma & 0 \end{bmatrix} \begin{bmatrix} F_{bz} \\ M_{x+} \\ M_{y+} \end{bmatrix} + \begin{bmatrix} 0 & 0 \\ \gamma & 0 \\ 0 & \gamma \\ 0 & 0 \end{bmatrix} \begin{bmatrix} M_{x-} \\ M_{y-} \end{bmatrix} > 0$$

$$\gamma = 2c/\sigma \cong 2/r$$
(38)

As a consequence the horizontal components in Eqs. (26) and (27) hold

$$\mathbf{a}_{bx} = P \begin{bmatrix} a_{bx} \\ a_{by} \end{bmatrix} = b_m J_x^{-1} \mathbf{M}_x, \ b_m(t) = \frac{J_x(t) s}{2 m(t) \sigma} > 0$$
(39)

Assuming that the landing body is near-cylindrical (free of front shield and back-shell), with radius $r_b \cong r \cong 2$ m and height $h_b = \rho r$, $\rho < \sqrt{2}$, the coefficient b_m becomes

$$b_m(t) \approx \rho^2 \operatorname{rtan}\beta/24 < 0.05 \text{ m}$$
 (40)

which shows that b_m can be kept as a constant in the presence of a variable mass m by an appropriate layout and use of the propellant tanks. Then assuming the following bound to the commanded angular acceleration (see Fig. 5).

$$\mid J_x^{-1} \mathbf{M}_x \mid \leqslant 1 \text{ rad/s}^2 \tag{41}$$

proves that

$$\mid$$
 B_z(θ) $a_{bx}(t) \mid \leq 0.02 \text{ m/s}^2 \ll g$ (42) as anticipated in the Theorem 1.1 proof.

1.5.2 Combined dynamics

Using Eqs. (27), (34) and (39), and defining the commanded angular acceleration u_x as follows:

$$\mathbf{u}_{x}(t) = \frac{\mathbf{a}_{q}}{b_{m}}(t) = \frac{1}{b_{m}}(\mathbf{S}(\mathbf{q})\,\mathbf{a}_{bx}(t) + \mathbf{d}_{x}(t)) \tag{43}$$

one finds that

$$\mathbf{d}_{q}(t) = b_{m}(\mathbf{\alpha}_{x} - \mathbf{d}_{m}(t)) = b_{m}\mathbf{u}_{x}$$

$$\mathbf{d}_{m}(t) = -\frac{\mathbf{d}_{x}(t)}{b_{m}} + J_{x}^{-1}S(\mathbf{\theta})\mathbf{M}_{dx} + \mathbf{m}_{x}(\mathbf{\theta}, \mathbf{\omega}_{b})$$
(44)

Finally the attitude command holds

$$\mathbf{\alpha}_{x} = \mathbf{u}_{x} + \mathbf{d}_{m} \tag{45}$$

The combined horizontal CoM and attitude dynamics is

$$\begin{bmatrix} \dot{\boldsymbol{x}} \\ \dot{\boldsymbol{v}}_{x} \\ \dot{\boldsymbol{q}} \\ \dot{\boldsymbol{\omega}}_{x} \end{bmatrix} (t) = \begin{bmatrix} 0 & I & 0 & 0 \\ 0 & 0 & a_{bx} (\boldsymbol{q}, t) I & 0 \\ 0 & 0 & 0 & I \\ 0 & 0 & 0 & 0 \end{bmatrix} \begin{bmatrix} \boldsymbol{x} \\ \boldsymbol{v}_{x} \\ \boldsymbol{q} \\ \boldsymbol{\omega}_{x} \end{bmatrix} (t) + \begin{bmatrix} 0 \\ b_{m}I \\ 0 \\ I \end{bmatrix} \boldsymbol{u}_{x}(t) + \begin{bmatrix} 0 \\ 0 \\ 0 \\ I \end{bmatrix} \boldsymbol{d}_{m}(t)$$

$$(46)$$

where the time varying gain $a_{lz} > 0$ is a function of q because of Eq. (28). Notice that the horizontal components x and y in Eq. (21) are decoupled except for the gain $c(t) = c_{\varphi}c_{\theta}$ entering a_{lz} . A similar equation is in Ref. [16] but with $b_m = 0$.

Eq. (46) must be completed with the vertical and spin dynamics from Eqs. (25) and (23).

Lemma 1.3 Eq. (46) is input-state linearized except for the gain a_{bz} (\mathbf{q} , t), and b_m (t) I. They produce two pairs of imaginary zeros.

$$z_{1,2} = z_{3,4} = \pm j\omega_{bz}$$

$$\omega_{bz} = \sqrt{a_{bz}(t)/b_m} \geqslant 6 \text{ rad/s(1 Hz)}$$

$$\frac{a_{bz}(t)}{b_m} = \frac{u_z(t) + g(1-\delta)}{c(t)b_m}$$

$$(47)$$

in the transfer function from angular to CoM acceleration. The zeros tend to be infinite for $\beta \rightarrow 0$ (axial thrusters). The zeros tend to vary only because of the vertical acceleration u_z and of c in Eq. (24).

Fig. 2 shows the combined horizontal dynamics, together with vertical and spin dynamics. Clouds denote unknown disturbance, to be modeled as stochastic signals and to be disturbance observer^[18,20]. estimated by Interconnections that are cancelled by the control law (known disturbance rejection) are not indicated. The most important interconnection is the axial acceleration $a_{bz} > 0$. A further interconnection generating a loop via vertical and horizontal control is c(t) > 0.

2 Descent control design

2.1 Guidance and navigation

CoM and attitude guidance are not treated

here, but following the embedded model control^[18-19,21] they are computed on the same Eq. (46) free of disturbances^[24]. Vertical and horizontal guidance are separated. The descent phase duration t_f is fixed by the vertical guidance. At $t=t_f$ the landing phase starts, depending on the touch-down mechanism. In the first three cases (past Mars missions and Ref. [5]) thrusters are switched off at t_f . In the last case (MSL, [8,13]) thrusters hover the body until the payload touches the ground. Vertical guidance provides reference altitude \underline{z} , velocity \underline{v}_z and acceleration \underline{a}_z (reference variables are underlined). Given \underline{a}_z , $\underline{a}_{lz} = \underline{a}_z/(\cos \varphi \cos \underline{\theta})$ is computed.

Horizontal guidance minimizes the energy of the tilt angles $\underline{\varphi}, \underline{\theta}$. Optimization is constrained by the tilt bounds φ_{\max} , θ_{\max} , and is iterated for accommodating the nonlinear gain between \underline{a}_z and \underline{a}_{bx} . Here we assume that a reference trajectory is available for all the state variables in Eq. (46), namely \underline{x} , \underline{v}_x , \underline{q} , $\underline{\omega}_x$ together with a reference angular acceleration \underline{u}_x .

Navigation (see Ref. [22] for concepts and Monte Carlo runs), driven by accelerometers and gyros and updated by local sensors, has been extended to measure unknown disturbances like d_z in Eq. (26), d_m in Eq. (45) and M_{dz} in Eq. (34) (clouds in Fig. 2). The latter ones allow the control law to recover the parametric uncertainty

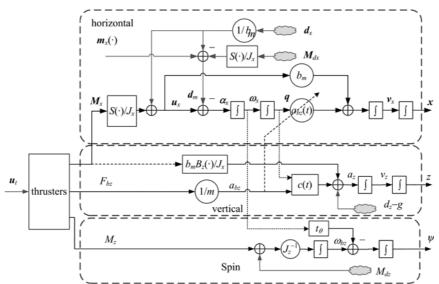


Fig. 2 Block-diagram of the overall linearized equations

affecting the known disturbance model. Each unknown disturbance is associated with a stochastic dynamics driven by noise^[20]. Noise estimation updates disturbance and controllable state variables as in Kalman filters. Disturbances in Eqs. (46), (34) and (26) are split into state, noise and known terms. A first order stochastic dynamics (random drift) is assumed, for the horizontal dynamics (46) as follows:

$$d_m(t) = x_m(t) + w_m(t) + m_x(\bullet)$$

$$\dot{x}_m(t) = w_d(t)$$
(48)

as well for the vertical CoM dynamics in Eq. (26) and the spin dynamics in Eq. (34).

$$d_{z}(t) = x_{d}(t) + w_{z}(t)$$

$$\dot{x}_{d}(t) = w_{dz}(t)$$

$$M_{dz}(t)/J_{z} = x_{mz}(t) + w_{mz}(t)$$

$$\dot{x}_{mr}(t) = w_{dmr}(t)$$

$$(49)$$

All the noise vectors \mathbf{w}_m and \mathbf{w}_d in Eq. (48) and \mathbf{w}_z , \mathbf{w}_{dz} , \mathbf{w}_{mz} and \mathbf{w}_{dmz} in Eq. (49) are (statistically) bounded and zero mean. In the following $\mathbf{m}_x(\cdot) = 0$ and is included in $\mathbf{x}_m(t)$. The random drift state variables $\mathbf{x}_m(t)$, \mathbf{x}_d and \mathbf{x}_{mz} make the horizontal, vertical and spin dynamics not stabilizable. The only stabilization procedure is to measure and cancel the drifting variables. Indirect measurements, not treated here, are provided by noise estimators. They estimate in real-time the noise samples for driving a discrete-time version of Eqs. (48) and (49), as shown in Refs. [19-20, 22]. Then cancellation becomes feasible less a bounded error.

2, 2 Control law

Only horizontal dynamics is addressed.

2.2.1 Horizontal dynamics

Given a reference trajectory, control law aims to reject known and unknown disturbance, and to make the tracking error bounded. Bounded error corresponds to internal stability. Because of the incomplete input-to-state linearization of Eq. (46), an "extended" tracking error must be defined including disturbance variables. A single horizontal component is considered, exploiting the coordinate decoupling emerging from Eq. (46). Identity matrices in Eq. (46) are replaced by unit.

Denote the four-dimensioned controllable state in Eq. (46) with \mathbf{x}_c , the scalar disturbance variable in Eq. (48) with d_m , and the scalar command with u_x . Dropping m_x (•) as anticipated above, the corresponding equation is rewritten as

$$\dot{\mathbf{x}}_{c}(t) = \mathbf{A}(t) \, \mathbf{x}_{c}(t) + \mathbf{B}u_{x}(t) + \mathbf{H}d_{m}(t)
d_{m}(t) = x_{m}(t) + w_{m}(t)
\dot{x}_{m}(t) = -\epsilon x_{m} + w_{d}(t)$$
(50)

where matrices and vectors derive from Eq. (46) and hold

$$\mathbf{x}_{c} = \begin{bmatrix} x \\ v \\ q \\ \omega \end{bmatrix}, A = \begin{bmatrix} 0 & 1 & 0 & 0 \\ 0 & 0 & a_{bx}(\bullet) & 0 \\ 0 & 0 & 0 & 1 \\ 0 & 0 & 0 & 0 \end{bmatrix}$$

$$B = \begin{bmatrix} 0 \\ b_{m} \\ 0 \\ 1 \end{bmatrix}, H = \begin{bmatrix} 0 \\ 0 \\ 0 \\ 1 \end{bmatrix}$$
(51)

The unknown part of d_m has been written as the sum of a wide-band noise (white noise in discrete time) and a random drift x_m . Leaving $\epsilon \rightarrow 0$ makes x_m drift and diverge, thus forcing the design of a robust disturbance rejection. The "extended" tracking error is defined as

$$\underline{\boldsymbol{e}}_{c}(t) = \underline{\boldsymbol{x}}_{c}(t) - \boldsymbol{x}_{c}(t) - Q(t) x_{m}(t)$$
 (52)

where \underline{x}_c is the reference state and Q is a four-dimensional vector to be found. The output tracking error corresponds to position error and can be written as

$$\underline{e}_{y}(t) = \underline{C}\underline{e}_{c}(t)
C = \begin{bmatrix} 1 & 0 & 0 & 0 \end{bmatrix}$$
(53)

Following Eqs. (45), (34) and (44) the control law is found to be

$$u_x(t) = \underline{u}_x(t) + K(t)\underline{e}_c(t) - p(t)x_m(t)$$
 (54)
where $K(t)$ stabilizes $A(t) - BK(t)$, and $p(t)$ is a scalar to be found together with $Q(t)$.

As shown in Ref. [18] the unknown gains Q and p, weighting the disturbance state, are not to be designed like K, but they directly derive from Eq. (52) through the Sylvester matrix equation.

$$\begin{bmatrix} 0 \\ H + \dot{Q}(t) \end{bmatrix} = \begin{bmatrix} C & 0 \\ A(t) & B \end{bmatrix} \begin{bmatrix} Q(t) \\ p(t) \end{bmatrix}$$
 (55)

which has a solution if the system matrix in Eq. (55) has no zeros in the origin. The solution of Eq. (55) can be found to be

$$\begin{bmatrix} \mathbf{Q}(t) \\ p \end{bmatrix} = \begin{bmatrix} \mathbf{C} & 0 \\ \mathbf{A}(t) & \mathbf{B} \end{bmatrix}^{-1} \begin{bmatrix} 0 \\ \mathbf{H} + \dot{\mathbf{Q}}(t) \end{bmatrix}$$
 (56)

and

$$p(t) = 1 + \ddot{q}_{3}(t)$$

$$Q^{T}(t) = \begin{bmatrix} 0 & 0 & q_{3}(t) = -b_{m}/a_{bz}(t) & \dot{q}_{3}(t) \end{bmatrix}$$
(57)

As a result, attitude and angular rate tracking errors, i. e. the third and fourth component of e_c in Eq. (52), must include the disturbance state.

It is of interest to assess the value and bound of q_3 and of its derivatives in Eq. (57).

Lemma 2.1 $q_{\bar{s}}$ and the first and second derivatives are bounded if and only the vertical jerk \dot{u}_z , the vertical snap \ddot{u}_z , the angular rates $\dot{\varphi}$, $\dot{\theta}$ and the accelerations $\ddot{\varphi}$, $\ddot{\theta}$ are bounded.

Proof Firstly, using Eq. (32) and setting $\mu \cong \mu - \delta$, rewrite the bounded $q_3(t)$ as follows:

$$|q_3(t)| = \frac{b_m}{a_{bz}(t)} = \frac{b_m c(t)}{g(1+\mu)} < 0.005 \text{ s}^2$$
 (58)

Setting $\dot{u}_z \cong \dot{u}_z - g\dot{\delta}$ and $\ddot{u}_z \cong \ddot{u}_z - g\ddot{\delta}$ the first and second derivatives hold

$$|\dot{q}_{3}(t)| \cong |q_{3}(t)| \approx |q_{3}(t)| \approx$$

where f is a complex trigonometric function. Eqs. (58) and (59) prove the Lemma. \dot{u}_z and \dot{u}_z are bounded by guidance thrust slew rate, angular rates and accelerations.

The bounds in Eqs. (58) and (59) correspond to the following bounds employed by Monte Carlo simulations in Section 3.

$$\begin{vmatrix} \dot{u}_{z}/g(1+\mu) & | < 1 \text{ s}^{-1} \\ | \ddot{u}_{z}/g(1+\mu) & | < 1 \text{ s}^{-2} \\ | \theta |, | \varphi | \leqslant \pi/4 \\ | \dot{\theta} |, | \dot{\varphi} | \leqslant 1 \text{ rad/s}$$

$$| \ddot{\theta} |, | \ddot{\varphi} | \leqslant 1 \text{ rad/s}^{2}$$

$$(60)$$

In view of the second inequality in Eq. (49), the approximation p=1 in Eq. (57) has been adopted, which avoids \dot{q}_3 computation.

The following theorem provides the conditions for the tracking error to be bounded, notwithstanding the unbounded drift in Eqs. (48) and (49).

Theorem 2.1 Assume perfect knowledge of the parameters in Eq. (50) and that \underline{u}_x and \underline{x}_c satisfy Eq. (50) free of disturbance, i. e.

$$\underline{\dot{\mathbf{x}}}_{c}(t) = \underline{\mathbf{A}}(t)\,\underline{\mathbf{x}}_{c}(t) + \underline{\mathbf{B}}\underline{\mathbf{u}}_{x}(t)\,,\,\underline{\mathbf{A}}(t) = \mathbf{A}(t)\,,\,\underline{\mathbf{B}} = \mathbf{B}$$
(61)

Moreover, assume that w_m and w_d are bounded, and that u_x is affected by a bounded error Δu_x because of the navigation errors. The tracking error Eq. (52) is bounded if and only if K(t) asymptotically stabilizes $A_c(t) = A(t) - B(t) K(t)$ and Eq. (56) holds.

Proof Eq. (56) cancels the unknown and unbounded disturbance state x_m from the tracking error equation.

$$\frac{\dot{\underline{e}}_{c}(t) = A_{c}\underline{e}_{c}(t) - Hw_{m}(t) - Qw_{d}(t) - B\Delta u_{x}(t)}{\underline{e}_{y}(t) = C\underline{e}_{c}(t)}$$
(62)

Because A_c is asymptotically stable, and because w_m , w_d and Δu_x are bounded, Eq. (62) proves the sufficient condition. Asymptotical stability of $A_c(t)$ is necessary for Eq. (62) to be bounded-input-bounded-output. Eq. (56) is necessary to fully cancel the unbounded x_m from Eq. (62).

The next lemma is preliminary to Theorem 2.2.

Lemma 2.2 Given a Hurwitz polynomial with constant coefficients.

$$P(\lambda) = \lambda^4 + c_3 \lambda^3 + c_2 \lambda^2 + c_1 \lambda + c_0$$
 (63) a unique matrix $K^T = [k_1 \quad k_1 \quad k_3 \quad k_4]$ exists such that $P(\lambda)$ is the characteristic polynomial of A_c in Eq. (62).

Proof The feedback gains exist because $a_{bz} > 0$ and hold

$$k_1 = c_0/a_{bz}, k_2 = c_1/a_{bz} k_3 = c_2 - c_0 b_m/a_{bz}, k_4 = c_3 - c_1 b_m/a_{bz}$$
(64)

Since control performance is defined at the terminal time t_f , convergence of (62) as $t \rightarrow t_f$ is of interest.

Theorem 2.2 Under Theorem 2.1 and assuming $\Delta u_x \rightarrow 0$ for $t \rightarrow t_f$ and $a_{bx} \rightarrow \underline{a}_{bx}$ (constant), the expected value $E\{e_c(t_f)\}$ is bounded by an arbitrarily small value dependent on the eigenvalues of Eq. (63). A bound^[25] is

$$\ln\left(\frac{\mid E\{\underline{\boldsymbol{\varrho}}_{c}(t_{f})\}\mid}{\mid \underline{\boldsymbol{\varrho}}_{c}(0)\mid}\right) \leqslant \eta - \frac{t_{f}}{\tau_{\min}(A_{c})} + (m-1)\ln(t_{f})$$
(65)

which is dominated by the negative term for $\tau_{\min}(A_c) \ll t_f$. In Eq. (65) $\tau_{\min}(A_c)$ is the least time constant of A_c , m=4 and η depends on m and on the normalized eigenvector matrix of A_c .

Assuming $t_f > 30$ s and $\tau_{\min} \leq 5$ s, $E\{\underline{e}_{\epsilon}(t_f)\}$ quickly converges to zero for $t \rightarrow t_f$, and the only random deviations are due to w_m , w_d and Δu_x .

2. 2. 2 Control law tuning

Tuning of the gains in Eq. (64) is made by assuming that the navigation error Δu_x dominates w_m and w_d . To this end Δu_x can be expressed from Eq. (54) as

$$\Delta u_r(t) \cong K(t) \hat{\mathbf{e}}(t)$$
 (66)

i. e. as a combination of the vector $\hat{\boldsymbol{e}}$ of the state navigation errors. Assuming their covariance matrix \hat{S}^2_e is known, the tracking error covariance $\underline{S}^2_e(t) = E\{\underline{\boldsymbol{e}}_c(t)\underline{\boldsymbol{e}}_c^T(t)\}$ can be reduced below a target bound $S^2_{e,\max}(t_f)$ at the terminal time by tuning the gains in Eq. (64) or the relevant eigenvalues $\Lambda = \{\lambda_1, \dots, \lambda_4\}$. Theorem 2.1 makes it possible to replace $\underline{S}^2_e(t_f)$ with the steady state solution \underline{S}^2_e of the Lyapunov equation.

 $A(t_f) \underline{S}_e^2 + \underline{S}_e^2 A^T(t_f) + K(t_f) \hat{S}_e^2 K(t_f) = 0$ (67) Tuning has been done numerically assuming that Λ is defined by a single unknown eigenvalue as follows:

$$\Lambda = \{\lambda = -2\pi f_u, \lambda, \lambda/10, \lambda/10\}$$
 (68)

Partition of Eq. (68) into fast and slow eigenvalue pairs reflects the hierarchy between attitude and horizontal motion, as attitude must change faster to drive horizontal velocity and position to change.

Figs. 3 and 4 show the standard deviations obtained from the square root of the diagonal of \underline{S}_e^2 versus the design frequency f_u in Eq. (68). Attitude and horizontal velocity impose the solution because of the target. Performance is

given in terms of the absolute velocity v_f and of the body axial tilt q_f at the terminal time. They are defined as

$$\begin{vmatrix}
\mathbf{v}_f = (\mathbf{v}_x^{\mathsf{T}}(t_f)\mathbf{v}_x(t_f))^{1/2} \\
\mathbf{q}_f = (\mathbf{q}^{\mathsf{T}}(t_f)\mathbf{q}(t_f))^{1/2}
\end{vmatrix}$$
(69)

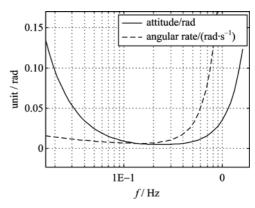


Fig. 3 Standard deviation of the attitude and angular rate errors

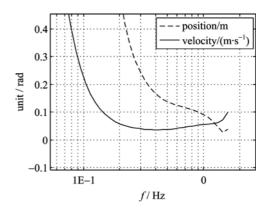


Fig. 4 Standard deviation of position and velocity errors

Tab. 1 reports the target max values, the a priori max values obtained from \underline{S}_e^2 and the a posteriori values computed from the Monte Carlo runs in Section 3. The designed frequency f_u has been selected to match a priori and target values, and is close to the minima of the tilt and velocity standard deviations in Figs. 3 and 4.

Tab. 1 Control law tuning and Monte Carlo results

| No. | parameter | symbol | unit | value |
|-----|------------------------------------|---------------|----------------|-------|
| 0 | Body axial tilt (max) | | rad | 0.02 |
| 1 | Absolute velocity (max) | | m/s | 0.5 |
| 2 | Designed frequency | f_u | Hz | 0.3 |
| 3 | A priori max tilt | $q_{f,\max}$ | rad | 0.02 |
| 4 | A priori max absolute velocity | $v_f,_{\max}$ | $\mathrm{m/s}$ | 0.17 |
| 5 | A posteriori max tilt | | rad | 0.015 |
| 6 | A posteriori max absolute velocity | y | m/s | 0.13 |

3 Simulated results

One hundred Monte Carlo runs have been performed under the following conditions. Mars atmosphere and winds, sensor and thruster noise, thruster dynamics, navigation errors (initial attitude error of about 0.02 rad), have been simulated. The main data and Monte Carlo initial conditions are in Tab. 2.

Tab. 2 Main data and Monte Carlo conditions

| No. | parameter | symbol | unit | value |
|-----|----------------------|---|------------------|---------------|
| 0 | Wet mass | m_0 | kg | 4000 |
| 1 | Inertia | $\int_{-\infty}^{\infty}$ | kgm^2 | 3000 |
| 2 | Inertia | \int_{-z} | kgm^2 | 5000 |
| 3 | Initial altitude | ≈0 | m | 4000 to 5000 |
| 4 | Vertical velocity | v ₂₀ | m/s | 80 to 120 |
| 5 | Horizontal speed | $\mid v_{x0} \mid$, $\mid v_{y0} \mid$ | m/s | €30 |
| 6 | Initial tilt | $(\varphi_0^2 + \theta_0^2)^{1/2}$ | rad | ≤ 0.35 |
| 7 | Initial angular rate | ω_{bx0} , ω_{by0} | $\mathrm{rad/s}$ | €0.05 |
| 8 | Control rate | f_c | Hz | 10 |
| 9 | Distance (radius) | $(x_l^2 + y_l^2)^{1/2}$ | m | €3500 |

Fig. 5 shows the ensemble of the commanded angular acceleration (yaw) during the first 10 s of the descent phase lasting 100 s. The pair of initial oscillations are necessary to recover wrong directions at the onset. They are the second derivative of the initial yaw peak in Fig. 6. After that, acceleration damps out into a band less than 0.1 rad/s².

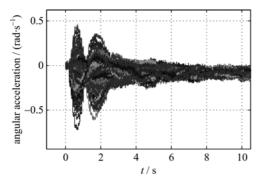


Fig. 5 Yaw commanded acceleration (enlargement)

Fig. 6 shows the ensemble of the Monte Carlo profiles for the yaw angle φ . Tilt versus altitude is in Fig. 8. After a first movement to correct initial conditions (the top sharp turn in Fig. 8), the tilt profile resembles the smooth shape of a bang-bang

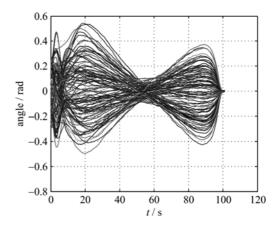


Fig. 6 Monte Carlo profiles of the yaw angle

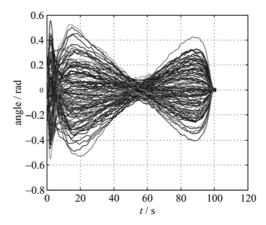


Fig. 7 Monte Carlo profiles of the pitch angle

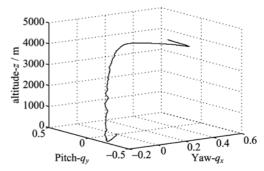


Fig. 8 Tilt versus altitude

acceleration: acceleration, coasting and braking. Zero terminal tilt is achieved in short time (the bottom sharp turn in Fig. 8). The peak value of 0.5 rad times $\sqrt{2}$ corresponds to the cone semi-aperture of $q_{\text{max}} = \pi/4$ in Eq. (60).

Fig. 9 shows the histograms from the 100 runs of the body axial tilt at $t=t_f$, defined in Eq. (69). Fig. 10 shows the histogram of the absolute horizontal velocity defined in Eq. (69). They meet target requirements in Tab. 1.

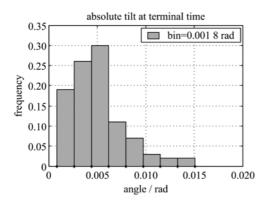


Fig. 9 Histogram of the axial tilt

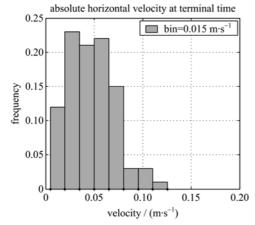


Fig. 10 Histogram the absolute horizontal velocity

4 Conclusion

The paper solves propulsion planetary descent using combined attitude and CoM dynamics, which is 4th order in the horizontal components. The combined dynamics is not input-state linearized which requires a specific control design and internal stability to be proved. Control design has been done and stability has been proved in the presence of external disturbances that are unbounded and not stabilizable. Monte Carlo runs show that the designed control is effective in reaching the expected terminal requirements when thrusters are switched off. Experimental test using a quadrotor is under development.

5 Appendix

The equations of flight of a body over a rotating planet are derived^[26]. The position vectors are defined as

$$\vec{r}_p = \overrightarrow{C_pO}, \ \vec{r}_l = \overrightarrow{OC} \tag{70}$$

and holds

$$\vec{r} = \vec{r}_{P} + \vec{r}_{l} = (r_{P} + z_{l})\vec{k}_{l} + x_{l}\vec{i}_{l} + y_{l}\vec{j}_{l}$$

$$\vec{r}_{l} = v_{lx}\vec{i}_{l} + v_{ly}\vec{j} + v_{lz}\vec{k}_{l},$$

$$\vec{v}_{l} = \dot{v}_{lx}\vec{i}_{l} + \dot{v}_{ly}\vec{j} + \dot{v}_{lz}\vec{k}_{l}$$

$$(71)$$

where r_p is fixed, $\overset{\rightarrow}{r_l}$ and $\overset{\rightarrow}{v_l}$ are derivatives in the local frame. The local-to-planet transformation R_l^p employs 2-1-3 Euler angles $\{\Lambda(t) + \lambda, -L, \chi\}$, where longitude λ , latitude L and heading χ refer to O and are fixed, whereas $\Lambda(t)$ accounts for the reference meridian rotation. Local coordinates ω_l of the planet rotation $\overset{\rightarrow}{\omega_p} = \omega_p \overset{\rightarrow}{j_p}$ hold

$$\boldsymbol{\omega}_{l} = (R_{l}^{p})^{-1} \begin{bmatrix} 0 \\ \omega_{p} \\ 0 \end{bmatrix} = \begin{bmatrix} s_{\chi}c_{L} \\ c_{\chi}c_{L} \\ s_{L} \end{bmatrix}$$

$$R_{l}^{p} = \begin{bmatrix} c_{\lambda} & -s_{\lambda}s_{L} & s_{\lambda}c_{L} \\ 0 & c_{L} & s_{L} \\ -s_{\lambda} & -c_{\lambda}s_{L} & c_{\lambda}c_{L} \end{bmatrix} \begin{bmatrix} c_{\chi} & -s_{\chi} & 0 \\ s_{\chi} & c_{\chi} & 0 \\ 0 & 0 & 1 \end{bmatrix}$$

$$(72)$$

The kinematic equations of \overrightarrow{r} is

$$\vec{r} = \vec{r}_l + \vec{\omega}_p \times (\vec{r}_p + \vec{r}_l)$$

$$\vec{r} = \vec{v}_l + \vec{\omega}_p \times (\vec{\omega}_p \times (\vec{r}_p + \vec{r}_l)) + 2\vec{\omega}_p \times \vec{r}_l$$
(73)

lead to the local state equations:

$$\mathbf{v}_{l}(t) = \dot{\mathbf{r}}_{l}(t), \ \mathbf{r}_{l}(0) = \mathbf{r}_{\mathbb{D}}$$

$$\dot{\mathbf{v}}_{l}(t) = \mathbf{F}_{l}(t)/m(t) - \mathbf{\omega}_{l} \times (\mathbf{\omega}_{l} \times (\mathbf{r}_{p} + \mathbf{r}_{l})) - 2\mathbf{\omega}_{l} \times \mathbf{v}_{l}$$

$$\dot{m}(t) = -p(t), \ m(0) = m_{0}, \ v_{l}(0) = v_{\mathbb{D}}$$
(74)

where local coordinates \mathbf{r}_l , \mathbf{v}_l and \mathbf{F}_l have been used for position, velocity and force, and the mass flow \dot{m} has been added. Separating gravity, thrust and aerodynamic forces, the second equation in Eq. (74) is rewritten as

$$\dot{\mathbf{v}}_{l}(t) = -\mathbf{g} + \mathbf{d}_{l}(t) + \mathbf{R}_{b}^{l}\mathbf{a}_{b}(t), \ \mathbf{g} = \begin{bmatrix} 0 & 0 & \mathbf{g} \end{bmatrix}^{\mathrm{T}}$$
(75)

where $g \cong 3$. 7 m/s² (Mars ground), \mathbf{d}_l includes aerodynamic forces and the kinematic accelerations in Eq. (74), and \mathbf{a}_b denotes the thrust acceleration in the body frame. Eq. (75) can be seen as the flat planet approximation of the planetary entry

equations[26].

Acknowledgments Part of the work of the authors from Politecnico di Torino has been funded by Regione Piemente in the frame of a technological research program.

References

- [1] Citron S J, Dunin S E, Meissinger H F. A terminal guidance technique for lunar landing [J]. AIAA Journal, 1964, 2(3): 503-509.
- [2] McInnes C R. Path shaping guidance for terminal lunar descent[J]. Acta Astronautica, 1995, 36(7): 367-377.
- [3] McInnes C R. Direct adaptive control for gravity-turn descent [J]. Journal of Guidance Control and Dynamics, 1999, 22(2): 373-375.
- [4] Hablani H B. Interplanetary spacecraft controllers using thrusters[J]. Journal of Guidance Control and Dynamics, 1998, 21(4): 542-550.
- [5] Martella P, Buonocore M, Canuto E, et al. Design and verification of the GNC for the European ExoMars EDL demonstrator [C]// AIAA Guidance, navigation and control conference. Portland, USA, 2011, AIAA 2011-6341(1-25).
- [6] de LaFontaine J, Neveu D, Lebel K. Autonomous planetary landing with obstacle avoidance: The quartic polynomial guidance revisited [J]. Advances in Astronautical Sciences, 2004, 119(3): 2717-2742.
- [7] Wong E C, Singh G, Masciarelli J P. Guidance and control design for hazard avoidance and safe landing on Mars[J]. Journal of Spacecraft and Rockets, 2006, 43(2): 378-384.
- [8] Singh G, SanMartin A M, Wong E C. Guidance and control design for powered descent and landing on Mars [C]// Aerospace Conference. IEEE Press, 2007: 1-8.
- [9] Najson F, Mease K D. Computationally inexpensive guidance algorithm for fuel-efficient terminal descent [J]. Journal of Guidance, Control and Dynamics, 2006, 29(4): 955-964.
- [10] Sostaric R R, Rea J R. Powered descent guidance methods for the Moon and Mars [C]// AIAA Guidance, Navigation, and Control Conference. San Francisco, USA: IEEE Press, 2005, 4: 4 495-4 514.
- [11] Ploen S R, Acikmese A B, Wolf A. A comparison of powered descent guidance laws for Mars pinpoint landing [C]// AIAA/AAS Astrodynamics Specialist Conference and Exhibit. Keystone, USA, 2006: AIAA 2006-6676(1-16).
- [12] Grant M J, Steinfeldt B A, Braun R, et al. Smart

- divert: A new Mars robotic entry, descent, and landing architecture [J]. Journal of Spacecraft and Rockets, 2010, 47(3): 385-393.
- [13] Way D W, Powell R W, Chen A, et al. Mars Science Laboratory: Entry, descent and landing system performance [C]// Aerospace Conference. Big Sky, USA: IEEE Press, 2007: 1-19.
- [14] de Lafontaine J, Neveu D, Lebel K. Autonomous planetary landing using a LIDAR sensor: The closed-loop system[C]// 6th International ESA Conference on Guidance, Navigation and Control Systems. Loutraki, Greece: IEEE Press, 2006: ESA SP-606(3.1-3.10).
- [15] Huang X Y, Cui H T, Cui P Y. Autonomous optical navigation and guidance for soft landing on asteroids [J]. Acta Astronautica, 2004, 54(10): 763-771.
- [16]Guerrero J A, Castillo P. Trajectory tracking for a group of mini rotorcraft flying in formation[C]// 18th IFAC Word Congress. Milan, Italy, 2011; 6 331-6 336.
- [17] Slotine J J E, Li W P. Applied Nonlinear Control[M]. Prentice-Hall, 1991.
- [18] Canuto E. Embedded model control: Outline of the theory[J]. ISA Transactions, 2007, 46(3): 363-377.
- [19] Canuto E, Acuna-Bravo W, Molano-Jimenez A, et al. Embedded Model Control calls for disturbance modeling and rejection[J]. ISA Transactions, 2012, 51(5): 584-595.
- [20] Canuto E, Molano A, Massotti L. Drag-free control of the GOCE satellite: Noise and observer design [J]. IEEE Transactions on Control Systems Technology, 2010, 18(2): 501-509.
- [21] Canuto E. Drag-free and attitude control for the GOCE satellite[J]. Automatica, 2008, 44(7): 1 766-1 780.
- [22] Canuto E, Molano-Jimenez A, Perez-Montenegro C. Disturbance rejection in space applications: Problems and solutions[J]. Acta Astronautica, 2012, 72: 121-131.
- [23] Canuto E, Molano-Jimenez A, Perez-Montenegro C, et al. Long-distance, drag-free, low-thrust, LEO formation control for Earth gravity monitoring [J]. Acta Astronautica, 2011,69(7-8):571-582.
- [24] Canuto E, Molano-Jimenez A, Acuna-Bravo W. Propulsive guidance and control for planetary landing [C]//Proceedings of the 5th International Conference on Astrodynamics Tools and Techniques, ESA/ESTEC. The Netherlands, 2012; 8. 3. 1-8. 3. 8.
- [25] van Loan C. The sensitivity of the matrix exponential [J]. SIAM Journal of Numerical Analysis, 1977, 14(6): 971-981.
- [26] Vinh N X. Optimal Trajectories in Atmospheric Flight M. Amsterdam; Elsevier, 1981.